Hindawi
Wireless Communications and Mobile Computing
Volume 2017, Article ID 9628565, 10 pages
https://doi.org/10.1155/2017/9628565

WILEY | Hindawi

Research Article

Performance Analysis of Three-Dimensional Clustered Device-to-Device Networks for Internet of Things

Haejoon Jung[1] and In-Ho Lee[2]

[1]*Department of Information and Telecommunication Engineering, Incheon National University, Incheon 22012, Republic of Korea*
[2]*Department of Electrical, Electronic and Control Engineering, Hankyong National University, Anseong 17579, Republic of Korea*

Correspondence should be addressed to In-Ho Lee; ihlee@hknu.ac.kr

Received 27 April 2017; Accepted 10 September 2017; Published 13 November 2017

Academic Editor: Haiyu Huang

Internet of things (IoT) is a smart technology that connects anything anywhere at any time. Intelligent device-to-device (D2D) communication, in which devices will communicate with each other autonomously without any centralized control, is an integral part of the Internet of Things (IoT) ecosystem. Thus, for D2D applications such as local file sharing or swarm sensing, we study communications between devices in proximity in ultra-dense urban environments, where devices are stacked vertically and dispersed in the horizontal plane. To reflect the spatiotemporal correlation inherently embedded in the D2D communications, we model and analyze clustered D2D networks in three-dimensional (3D) space based on Thomas cluster process (TCP), where the locations of clusters follow Poisson point process, and cluster members (devices) are normally distributed around their cluster centers. We assume that multiple device pairs in the network can share the same frequency band simultaneously. Thus, in the presence of cochannel interference from both the same cluster and the other clusters, we investigate the coverage probability and the area spectral efficiency of the clustered D2D networks in 3D space.

1. Introduction

Fifth-generation (5G) networks are being developed to support dramatically increasing data traffic with various multimedia applications [1]. As more devices are embraced to connect everything, everywhere, and everyone, networks become dense with unprecedented rise of mobile traffic. In this context, device-to-device (D2D) communication, which relieves the burden of base stations (BSs), is an important feature for various types of mobile networks in the future cellular systems [2–4]. Through the D2D communication, wireless devices can constantly interact to each other as well as with their environments, which is the key 5G enabler for the Internet of Things (IoT) [5–7]. The D2D communications to create, gather, and share information involve various types of devices such as sensors, smartphones, cars, health care gadgets, and home appliances [8].

Motivated by such emerging applications of the D2D communications, in this paper, we model and analyze D2D networks in three-dimensional (3D) space based on stochastic geometry [9]. To be specific, we consider 3D multicluster D2D networks, where devices in close proximity form a clustered network architecture. Poisson point process (PPP) is a widely used to analyze various types of networks (e.g., [10, 11]) including D2D networks, for its mathematical tractability. However, it cannot capture the fact that a device typically has multiple proximate devices, any of which is a potential serving device, with correlation in space and time.

To overcome this limitation, the authors in [12] develop a more realistic model for two-dimensional (2D) D2D networks, where the devices locations are modeled as a Poisson cluster process, in particular a variant of a Thomas cluster process [9], where the D2D network consists of multiple clusters, and cluster members (devices) are normally distributed around the center of clusters. Different from the widely used uniform spatial distribution assumption with PPP as in [13], the model proposed in [12] reflects the spatiotemporal correlation in the content demand in D2D networks in the IoT environments as indicated in [14, 15]. Using this model, they investigate 2D clustered D2D networks for local information sharing with each cluster [16–18].

However, as highlighted in [19–22], a 2D space model assumed in [12] may not be suitable for dense urban environments with high-rise buildings, where both devices and small-cell BSs are distributed over the 3D space. In [12], the coverage probability of wireless networks has been studied for various 2D deployment scenarios without much consideration for the vertical component of node distributions. However, to better model the future wireless environments (especially for the IoT applications) with ultra-dense deployments of devices and BSs, we need to consider the spatial distribution in the vertical space as well as the horizontal plane, as noted in [19–22]. For this reason, we extend the analytic framework of [12] in 2D space (on the horizontal plane) into 3D space. To our knowledge, this is the first study to model 3D D2D networks using TCP.

The contributions of this paper are fourfold. First, we derive the probability distributions of distance between two devices that belong to (i) the same cluster and (ii) two different clusters in the 3D space. Second, we provide the exact mathematical expressions of the coverage probability and the area spectral efficiency of the 3D clustered D2D networks. Third, the approximate upper and lower bounds of the coverage probability are obtained, which are useful in the coverage analysis to gain insights into system design guidelines. Moreover, we present numerical and simulation results to validate our analysis and compare the 2D and 3D TCP models with various system parameters.

2. System Model

We consider a D2D network in 3D space, where the devices participating communications exist in clusters by the nature of D2D communications [12]. We assume that each device communicates with other devices in the same cluster, while the devices across clusters do not communicate directly (or, the intercluster communications may use orthogonal channels). As shown in Figure 1, the locations of the devices in 3D space are modeled by a TCP, where the cluster centers follow a homogeneous PPP Φ_c with density λ_c. Also, the cluster members (devices) are independent and identically distributed (i.i.d.) according to a symmetric normal distribution with variance σ^2 around each cluster center $x \in \Phi_c$ with the density function of the device locations $y \in \mathbb{R}^3$ relative to a cluster center as

$$f_Y(y) = \frac{1}{(2\pi)^{3/2}\sigma^3} \exp\left(-\frac{\|y\|^2}{2\sigma^2}\right), \tag{1}$$

where σ is the scattering parameter.

The devices in the cluster of $x \in \Phi_c$ are denoted by $\mathcal{N}^x$, which has two subsets: (i) transmitting devices $\mathcal{N}_t^x$ and (ii) receiving devices $\mathcal{N}_r^x$. Suppose the set of simultaneously transmitting devices in the cluster is $\mathcal{B}^x \subseteq \mathcal{N}_t^x$, and its cardinality $|\mathcal{B}^x|$ follows a Poisson distribution with mean λ_t. In other words, the number of simultaneously active transmitting devices (Dev-Txs) inside each cluster is a Poisson random variable (RV) with mean λ_t. Therefore, excluding the serving (or desired) Dev-Tx, we assume that the number of interfering devices follows a Poisson distribution with mean

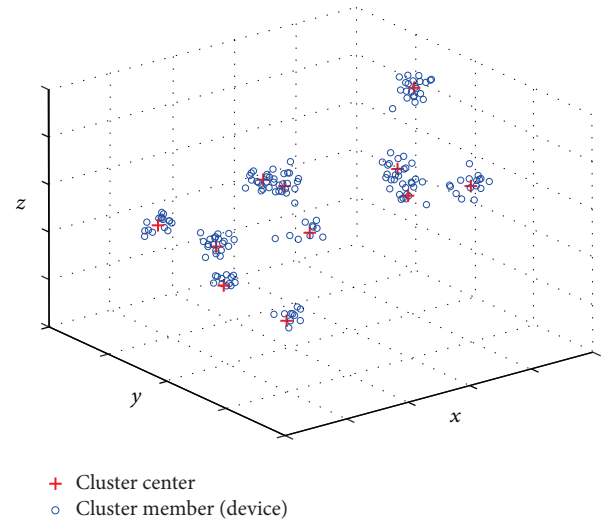

Figure 1: An example illustration of a three-dimensional clustered D2D network based on TCP.

$(\lambda_t - 1)$. As in [12], without loss of generality, we perform analysis based on a typical device in a representative cluster $x_0 \in \Phi_c$, where the typical device is regarded as the device receiver of interest. We assume that the typical device is located at the origin.

We assume that the serving Dev-Tx is located at y_0 inside the cluster $x_0 \in \Phi_c$. Thus, the distance between the serving Dev-Tx and the typical device is denoted by $r = \|y_0 + x_0\|$. Hence, with the transmit power of each device denoted by P_0, the received power at the typical device is

$$S = P_0 h_0 r^{-\alpha} = \frac{P_0 h_0}{\|x_0 + y_0\|^\alpha}, \tag{2}$$

where α is the path-loss exponent and h_0 is the power gain of small scale fading channel, which follows exponential distribution with unit mean, as in [12, 19–21]. The typical device suffers from two types of cochannel interference: (i) intracluster interference caused by the simultaneously active Dev-Txs in the same cluster and (ii) intercluster interference caused by the Dev-Txs in the other clusters, which are represented as

$$I_{\text{intra}} = \sum_{y \in \mathcal{B}^{x_0} \setminus y_0} \frac{P_0 h_{y_{x_0}}}{\|x_0 + y\|^\alpha}, \tag{3}$$

$$I_{\text{inter}} = \sum_{x \in \Phi_c \setminus x_0} \sum_{y \in \mathcal{B}^x} \frac{P_0 h_{y_x}}{\|x + y\|^\alpha}, \tag{4}$$

respectively. Consequently, assuming interference-limited networks, the signal-to-interference-ratio (SIR) at the typical device is

$$\begin{aligned} \mathtt{SIR}(r) &= \frac{S}{I_{\text{intra}} + I_{\text{inter}}} \\ &= \frac{h_0 / \|x_0 + y_0\|^\alpha}{\sum_{y \in \mathcal{B}^{x_0} \setminus y_0} \left(h_{y_{x_0}} / \|x_0 + y\|^\alpha\right) + \sum_{x \in \Phi_c \setminus x_0} \sum_{y \in \mathcal{B}^x} \left(h_{y_x} / \|x + y\|^\alpha\right)}, \end{aligned} \tag{5}$$

where P_0 is canceled, since we assume the fixed transmit power for all Dev-Txs.

3. Distance Distributions

In this section, we derive the probability distributions of the distances from the typical device to intra- and intercluster devices for system performance analysis associated with SIR. We assume that the content of interest for a typical device in a given cluster is available at a device chosen uniformly at random in the cluster, as in [12]. Based on this assumption, we derive the distance distributions from the typical device to the serving Dev-Tx, intra- and intercluster interferers.

3.1. Distances between Typical Device and Intracluster Dev-Txs. For the intracluster devices, let $\mathscr{D}_t^{x_0}$ be the set $\{D_i\}_{i=1:|\mathscr{N}_t^{x_0}|}$ of distances from the typical device to the set of possible Dev-Txs $\mathscr{N}_t^{x_0}$ in the cluster $x_0 \in \Phi_c$, where $d_i = \|x_0 + y\|$ is the realization of D_i. We note that the index i will be omitted when it is clear from the context. To delve into the distance statistics of D2D links, we first derive the probability distribution function (PDF) of the distance $v_0 = \|x_0\|$ between the cluster center x_0 and the typical device at the origin. Then, using this result, the PDF of the separation between the intracluster Dev-Tx and the typical device will be derived.

Lemma 1 (probability distribution of $v_0 = \|x_0\|$). *The PDF of v_0 is given by*

$$f_{v_0}(x) = \sqrt{\frac{2}{\pi}}\frac{x^2}{\sigma^3}\exp\left(-\frac{x^2}{2\sigma^2}\right), \tag{6}$$

where $x \geq 0$.

Proof. Based on the 3D Gaussian distribution defined in (1), $Z = v_0^2/\sigma^2$ is the squared sum of three i.i.d. standard (zero mean and unit variance) Gaussian random variables, which corresponds to the PDF as

$$f_Z(z) = \sqrt{\frac{z}{2\pi}}e^{-z/2}, \tag{7}$$

where $z \geq 0$. Therefore, by the change of variables, we can obtain the PDF in (6). □

Lemma 2 (probability distribution of $D = \|x_0 + y\|$). *The PDF of the separation between the typical device and the Dev-Tx in the same cluster is given by*

$$f_D(d) = \frac{d^2}{2\sqrt{\pi}\sigma^3}\exp\left(-\frac{d^2}{4\sigma^2}\right), \tag{8}$$

where $d \geq 0$.

Proof. The locations of the cluster center x_0 and the Dev-Txs y are i.i.d. random vectors in $\mathbb{R}^3$, where the three components follow i.i.d. Gaussian distributions with zero mean and variance of σ^2. Suppose $Z = \|x_0 + y\|^2/2\sigma^2$, which is the squared sum of three i.i.d standard Gaussian random variables. Thus, Z follows a chi-squared distribution with 3 degrees of freedom with the PDF:

$$f_Z(z) = \sqrt{\frac{z}{2\pi}}e^{-z/2}. \tag{9}$$

Therefore, the PDF of $D = \sigma\sqrt{2Z}$ in (8) can be derived by the change of variables (it is noted that the PDF and conditional PDF of D are, resp., obtained by extending the probability distribution analysis in 2D to 3D space). □

3.2. Conditional Distribution of D Given $\|x_0\|$. The distances of the typical device to the Dev-Txs in the same clusters, which are required to calculate S and I_{intra} in SIR, are correlated because of the common factor x_0. Therefore, conditioning the relative location of the cluster center, x_0, to typical device, we can treat the locations of the intracluster devices as i.i.d. RVs, which means that the distances between the typical device and the intracluster devices are i.i.d. To exploit this property, the following lemma gives the conditional distribution of D given $\|x_0\|$.

Lemma 3 (conditional probability distribution of $D = \|x_0 + y\|$ given $\|x_0\|$). *The conditional PDF of D for a given $\|x_0\|$ is derived as*

$$f_D(d \mid v_0) = \frac{d^{3/2}}{\sigma^2\sqrt{v_0}}e^{-(v_0^2+d^2)/2\sigma^2}I_{1/2}\left(\frac{v_0 d}{\sigma^2}\right), \tag{10}$$

where $d \geq 0$ and $I_{1/2}(t) = \sum_{k=0}^{\infty}(1/k!\Gamma(t+k+1))(t/2)^{1/2+2k}$ is the modified Bessel function with order $1/2$.

Proof. Let $Z = \|x_0 + y\|^2/\sigma^2$. Because $\|y\|^2/\sigma^2$ is the squared sum of three i.i.d standard Gaussian RVs, conditioned on $v_0 = \|x_0\|$, Z follows a noncentral chi-square distribution with the PDF:

$$f_Z(z \mid v_0) = \frac{1}{2}\left(\frac{\sigma^2 z}{v_0^2}\right)^{1/4}e^{-(v_0^2+\sigma^2 z)/2\sigma^2}I_{1/2}\left(\frac{v_0\sqrt{z}}{\sigma}\right). \tag{11}$$

Since $D = \|x_0 + y\| = \sigma\sqrt{Z}$, its PDF in (10) can be obtained by the change of variables (it is noted that the PDF and conditional PDF of D are, resp., obtained by extending the probability distribution analysis in 2D to 3D space). □

3.3. Distances to Serving Dev-Tx and Interferers: r, w, and u. Let the distances from the typical device to the serving Dev-Tx and intracluster interferer be $r = \|x_0 + y_0\|$ and $w = \|x_0 + y\|$, respectively. Their conditional PDFs given that $v_0 = \|x_0\|$ are same as (10). In other words, $f_R(r \mid v_0) = f_D(r \mid v_0)$ and $f_W(w \mid v_0) = f_D(w \mid v_0)$. In addition, conditioned on the distance $v = \|x\|$ between one of the other clusters $x \in \Phi_c$ and the typical device, the distances $\{u = \|x + y\|,\ \forall y \in \mathscr{B}^x\}$ between the typical device and the intercluster interfering Dev-Txs in $x \in \Phi_c$ are i.i.d., following the conditional PDF $f_U(u \mid v) = f_D(u \mid v_0 = v)$ given in (10). Also, the PDF of $v = \|x\|$ is identical to the PDF of $v_0 = \|x_0\|$ defined in (6).

4. Performance Analysis: $\mathtt{P_c}$ and ASE

In this section, we investigate the coverage probability, $\mathtt{P_c}$, and the area spectral efficiency, ASE, of the clustered D2D network. We first find the Laplace transforms of the two interference terms to characterize SIR. Then, we derive the exact expressions of $\mathtt{P_c}$ and ASE.

4.1. Laplace Transform of Intracluster Interference. Conditioned on $v_0 = \|x_0\|$, we first derive the Laplace transform of I_{intra} as

$$\begin{aligned}
\mathscr{L}_{I_{\text{intra}}}(s \mid v_0) &= \mathbb{E}\left[e^{-sI_{\text{intra}}}\right] \\
&= \mathbb{E}\left[\prod_{y\in\mathscr{B}^{x_0}\setminus y_0} \mathbb{E}_{h_{y_{x_0}}}\left[\exp\left(\frac{-sh_{y_{x_0}}}{\|x+y\|^{\alpha}}\right)\right]\right] \\
&\overset{(a)}{=} \mathbb{E}_{\mathscr{B}^{x_0}}\left[\prod_{y\in\mathscr{B}^{x_0}\setminus y_0} \frac{1}{1+s\|y+x_0\|^{-\alpha}}\right] \\
&\overset{(b)}{=} \exp\left((1-\lambda_t)\int_{\mathbb{R}^3} \frac{s\|y+x_0\|^{-\alpha}}{1+s\|y+x_0\|^{-\alpha}} f_Y(y)\,dy\right) \\
&\overset{(c)}{=} \exp\left((1-\lambda_t)\int_0^{\infty} \frac{sw^{-\alpha}}{1+sw^{-\alpha}} f_W(w \mid v_0)\,dw\right),
\end{aligned} \tag{12}$$

where (a) follows from the exponentially distributed h_{x_0} with unit mean and (b) follows from the probability generating functional (PGF) of Poisson process of the intracluster interferers with mean $(\lambda_t - 1)$. Also, (c) follows from $w = \|x_0 + y\|$.

4.2. Laplace Transform of Intercluster Interference. The Laplace transform of I_{inter} is given by

$$\begin{aligned}
\mathscr{L}_{I_{\text{inter}}}(s) &= \mathbb{E}\left[e^{-sI_{\text{inter}}}\right] \\
&= \mathbb{E}_{\Phi_c}\left[\prod_{x\in\Phi_c\setminus x_0} \mathbb{E}_{\mathscr{B}^x}\left[\prod_{y\in\mathscr{B}^x} \mathbb{E}_{h_{y_x}}\left[\exp\left(\frac{-sh_{y_x}}{\|x+y\|^{\alpha}}\right)\right]\right]\right] \\
&\overset{(a)}{=} \mathbb{E}_{\Phi_c}\left[\prod_{x\in\Phi_c\setminus x_0} \mathbb{E}_{\mathscr{B}^x}\left[\prod_{y\in\mathscr{B}^x} \frac{1}{1+s\|y+x\|^{-\alpha}}\right]\right] \\
&\overset{(b)}{=} \mathbb{E}_{\Phi_c}\left[\prod_{x\in\Phi_c\setminus x_0} \exp\left(\int_0^{\infty} \frac{-\lambda_t su^{-\alpha}}{1+su^{-\alpha}} f_U(u \mid v)\,du\right)\right] \\
&\overset{(c)}{=} \exp\left(4\pi\lambda_c \int_0^{\infty} (\kappa(v)-1)\,v^2 dv\right),
\end{aligned} \tag{13}$$

where $\kappa(v) = \exp(\int_0^{\infty}(-\lambda_t su^{-\alpha}/(1+su^{-\alpha}))f_U(u \mid v)du)$ and (a) follows from the exponentially distributed h_{x_0} with unit mean. Also, (b) and (c) follow from the PGF of Poisson process (with the mean of λ_c and $(\lambda_t - 1)$ resp.).

4.3. Coverage Probability and Area Spectral Efficiency. Letting β denote the SIR threshold for successful decoding at the receiver, which is a function of modulation and coding, the coverage probability is

$$\begin{aligned}
\mathtt{P_c} &= \mathbb{P}\left[\mathtt{SIR} > \beta\right] = \mathbb{E}_R\left\{\mathbb{P}\left[\mathtt{SIR}(R) > \beta \mid R\right]\right\} \\
&= \mathbb{E}_R\left\{\mathbb{P}\left[h_0 > \beta r^{\alpha}\left(I_{\text{intra}} + I_{\text{inter}}\right) \mid R = r\right]\right\} \\
&= \mathbb{E}_R\left\{\mathbb{E}\left\{e^{-\beta r^{\alpha}(I_{\text{intra}}+I_{\text{inter}})} \mid R = r\right\}\right\} \\
&= \int_0^{\infty}\int_0^{\infty} \mathscr{L}_{I_{\text{inter}}}(\beta r^{\alpha})\,\mathscr{L}_{I_{\text{intra}}}(\beta r^{\alpha} \mid v_0) \\
&\quad \times f_R(r \mid v_0)\, f_{v_0}(v_0)\,dr\,dv_0.
\end{aligned} \tag{14}$$

Therefore, letting the area spectral efficiency be defined as the average achievable rate per unit bandwidth per unit area as in [12], the area spectral efficiency is given by

$$\mathtt{ASE} = \lambda_t\lambda_c \log_2(1+\beta)\,\mathtt{P_c}, \tag{15}$$

where $\lambda_t\lambda_c$ is the average density of simultaneously active Dev-Txs of the whole D2D network.

5. Approximate Upper and Lower Bounds of $\mathtt{P_c}$

Because the exact expressions of $\mathtt{P_c}$ and ASE are unwieldy, we provide easy-to-compute upper and lower bounds of $\mathtt{P_c}$. In particular, the lower bound is in a closed form, which can be readily evaluated. As stated in Section 2, r and w are correlated because of the common factor x_0. For analytical tractability to derive the two approximate bounds, we allow separate deconditioning on r and w as in [12], which implies that r and w are i.i.d. following the PDF in (8).

5.1. Upper Bound of $\mathtt{P_c}$. Since the intracluster interferers are significantly closer to the typical device compared to the intercluster Dev-Txs, I_{intra} is dominant in the denominator of SIR. Thus, we can derive the approximate upper bound of SIR by ignoring I_{inter}, which corresponds to the upper bound of $\mathtt{P_c}$. By the i.i.d. assumption of r and w, the Laplace transform of I_{intra} can be approximated as $\widetilde{\mathscr{L}}_{I_{\text{intra}}}(s) = e^{(1-\lambda_t)\int_0^{\infty}(sw^{-\alpha}/(1+sw^{-\alpha}))f_W(w)dw}$, where $f_W(w)$ follows the PDF in (8). Thus, the upper bound of $\mathtt{P_c}$ is given by

$$\begin{aligned}
\widetilde{\mathtt{P_c}} &= \mathbb{E}_R\left\{\mathbb{P}\left[h_0 > \beta r^{\alpha} I_{\text{intra}} \mid R = r\right]\right\} \\
&= \int_0^{\infty} \widetilde{\mathscr{L}}_{I_{\text{intra}}}(\beta r^{\alpha})\, f_R(r)\,dr,
\end{aligned} \tag{16}$$

where $f_R(r)$ follows the PDF in (8).

5.2. Lower Bound of $\mathtt{P_c}$. We first derive lower bounds of $\mathscr{L}_{I_{\text{intra}}}(s)$ and $\mathscr{L}_{I_{\text{inter}}}(s)$ in closed forms. Then, using the two, the lower bound of $\mathtt{P_c}$ will be obtained.

Lemma 4 (lower bound of $\mathscr{L}_{I_{\text{intra}}}(s)$). *The lower bound on the Laplace transform of I_{intra} is*

$$\mathscr{L}_{I_{intra}}(s) \geq \mathscr{L}^{*}_{I_{intra}}(s) = \exp\left[\frac{1-\lambda_t}{6\sqrt{\pi}\sigma^3}\frac{s^{3/\alpha}(3\pi/\alpha)}{\sin(3\pi/\alpha)}\right]. \quad (17)$$

Proof. See Appendix A. □

Lemma 5 (lower bound of $\mathscr{L}_{I_{\text{inter}}}(s)$). *The lower bound on the Laplace transform of I_{inter} is given by*

$$\mathscr{L}_{I_{inter}}(s) \geq \mathscr{L}^{*}_{I_{inter}}(s) = \exp\left[-\frac{4}{3}s^{3/\alpha}\frac{\lambda_c\lambda_t\left(3\pi^2/\alpha\right)}{\sin(3\pi/\alpha)}\right]. \quad (18)$$

Proof. See Appendix B. □

With (17) and (18) along with the independent deconditioning assumption, we can obtain the approximate lower bound of $\mathtt{P}_c$ in a closed form as

$$\begin{aligned}\mathtt{P}_c &\geq \int_0^{\infty} \mathscr{L}^{*}_{I_{\text{inter}}}(\beta r^{\alpha})\,\mathscr{L}^{*}_{I_{\text{intra}}}(\beta r^{\alpha})\,f_R(r)\,dr \\ &\overset{(a)}{=} \int_0^{\infty} \exp\left(-\rho r^3\right)\frac{r^2}{2\sqrt{\pi}\sigma^3}\exp\left(-\frac{r^2}{4\sigma^2}\right)dr,\end{aligned} \quad (19)$$

where $\rho = (3\pi\beta^{3/\alpha}/\alpha\sin(3\pi/\alpha))((\lambda_t - 1)/6\sqrt{\pi}\sigma^3 + 4\pi\lambda_c\lambda_t/3)$ and (a) follows from $f_R(r)$ following (8). Because $\rho \geq 0$ ($\because \alpha \geq 2$ and $\lambda_t \geq 1$), we can obtain the lower bound in (20), where $\mathrm{Bi}(a) = (1/\pi)\int_0^{\infty}\cos(t^3/3 + at)dt$ is the Airy function, the derivative of which is $\mathrm{Bi}'(a)$. Moreover, ${}_2F_2$ is the generalized hypergeometric function [23].

$$\begin{aligned}&\mathtt{P}_c^{*} \\ &= \frac{108\rho^{4/3}\sigma^4\,{}_2F_2\left(1/2, 1; 1/3, 2/3; -1/432\rho^2\sigma^6\right) + e^{-1/864\rho^2\sigma^6}\left(3^{2/3}\pi\,\mathrm{Bi}\left(1/48\sqrt[3]{3}\rho^{4/3}\sigma^4\right) - 12\sqrt[3]{3}\pi\rho^{2/3}\sigma^2\mathrm{Bi}'\left(1/48\sqrt[3]{3}\rho^{4/3}\sigma^4\right)\right)}{648\sqrt{\pi}\rho^{7/3}\sigma^7}.\end{aligned} \quad (20)$$

6. Numerical Results

In this section, we present numerical results to validate our analysis and discuss the impacts of system parameters. For simulations, the device locations are randomly drawn from a TCP over $100 \times 100 \times 100\ \mathrm{m}^3$ cube. The cluster centers follow PPP with intensity λ_c, and devices are normally distributed around their cluster centers. Moreover, the number of the Dev-Txs in each cluster follows a Poisson distribution with mean λ_t. Also, we assume the path-loss exponent α of 4, as in [12, 19, 20]. The simulation results are obtained from 10^6 random realizations of device distribution (network topology) and Rayleigh fading channel.

6.1. Impacts of System Parameters. Figures 2(a) and 2(b) show how the coverage probability $\mathtt{P}_c$ varies, as the average number of simultaneously active Dev-Txs λ_t increases, with $\lambda_c = 0.3$ and 0.05, respectively. In the figures, the circles indicate the simulation results, while the solid line represents the theoretical results obtained numerically using (14). Moreover, the dash-dotted and dashed curves correspond to the upper and lower bounds $\widetilde{\mathtt{P}_c}$ and $\mathtt{P}_c{}^{*}$ in (16) and (20), respectively. In both figures, the simulation results show the excellent agreements with the theoretical results, which verifies our analysis. Moreover, the approximate upper and lower bounds of $\mathtt{P}_c$ derived in the previous section are validated. Specifically, comparing the two figures, when λ_c is large, the actual $\mathtt{P}_c$ is closer to the lower bound $\mathtt{P}_c{}^{*}$ compared to the upper bound $\widetilde{\mathtt{P}_c}$, as in Figure 2(a), because the large λ_c results in the higher intercluster interference I_{inter}, which is ignored in the $\widetilde{\mathtt{P}_c}$. On the other hand, for small λ_c, the gap between the exact $\mathtt{P}_c$ and its upper bound $\widetilde{\mathtt{P}_c}$ is significantly smaller compared to the difference from its lower bound $\mathtt{P}_c{}^{*}$, as in Figure 2(b), since the intracluster interference I_{intra} is dominant relative to the intercluster interference I_{inter}. In either case, the exact $\mathtt{P}_c$ curve is always bounded by $\widetilde{\mathtt{P}_c}$ and $\mathtt{P}_c{}^{*}$.

In Figures 3 and 4, we observe the impacts of σ and λ_c on exact $\mathtt{P}_c$, numerically obtained by (14), respectively. In the figures, we consider three scenarios in the presence of (i) only intracluster interference, (ii) only intercluster interference, and (iii) both intra- and intercluster interferences, which correspond to the dashed, dash-dotted, and solid lines, respectively. Moreover, the triangles and circles indicate the corresponding simulation results. In both figures, when λ_t grows, the intracluster interference, indicated by the dashed line, is dominant compared to the intercluster interference, which is indicated by the dash-dotted line. Also, in Figure 3, the larger σ, which means the larger spatial scattering of the devices from the cluster center, results in the lower $\mathtt{P}_c$. This can be attributed to the increased impact of I_{inter}, while the $\mathtt{P}_c$ curves only with I_{intra} do not change as indicated by the dashed curves in the figure. The $\mathtt{P}_c$ curves only with I_{intra} stay the same regardless of λ_t, because the variations of the serving and interfering Dev-Txs cancel each other. We can observe the same trend in Figure 4: as λ_c increases, $\mathtt{P}_c$ decreases because of the increased intercluster interference I_{inter}. On the other hand, the coverage probability $\mathtt{P}_c$ only with the intracluster interference I_{intra} does not vary under the variation in the cluster density λ_c.

Figures 5 and 6 show the exact area spectral efficiency ASE, numerically obtained by (15), versus the average number of simultaneously active Dev-Txs λ_t. In the figure, the horizontal axis indicates λ_t, while the vertical axis is ASE. Also, the solid, dashed, and dash-dotted lines represent the theoretical results with different system parameters (λ_c, σ, and β), while the circle and triangle markers represent the corresponding simulation results. Lastly, the optimal λ_t in each graph is indicated by the "x"-marker.

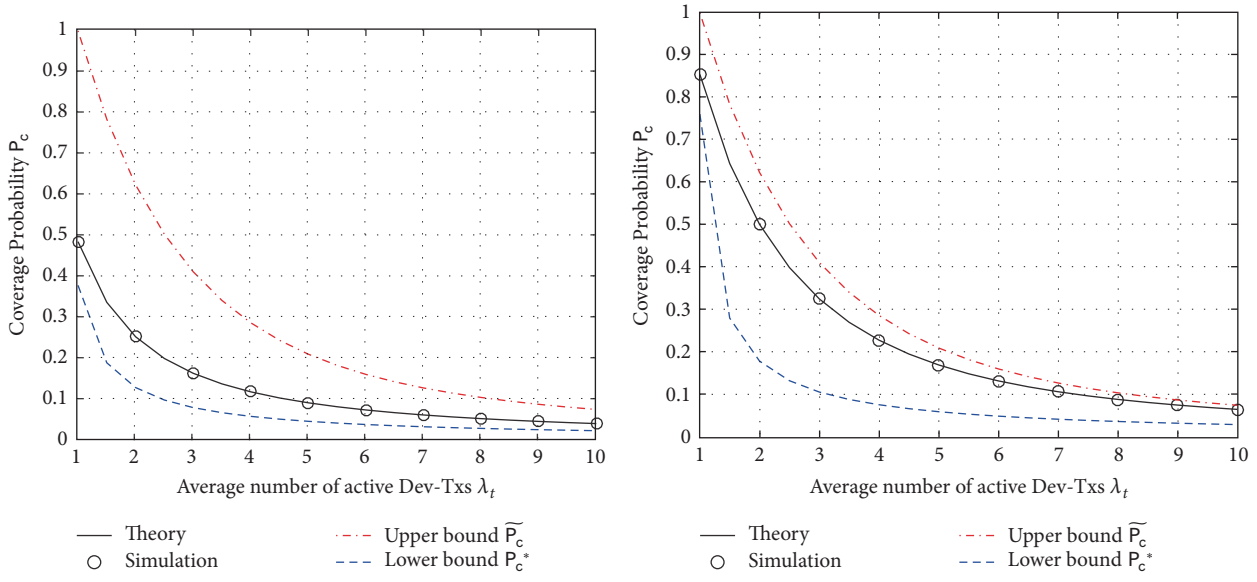

(a) P_c with $\lambda_c = 0.3$ clusters/m^3, $\sigma = 0.3$, and $\beta = 0$ dB

(b) P_c with $\lambda_c = 0.5$ clusters/m^3, $\sigma = 0.3$, and $\beta = 0$ dB

FIGURE 2: P_c versus λ_t: comparison with the upper and lower bounds.

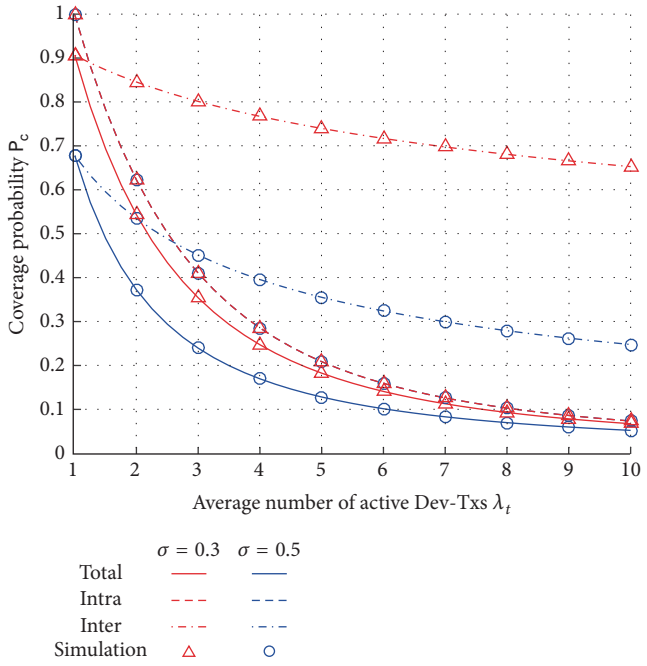

FIGURE 3: P_c versus λ_t with $\beta = 0$ dB, $\lambda_c = 0.03$ clusters/m^3, and $\sigma = \{0.3, 0.5\}$.

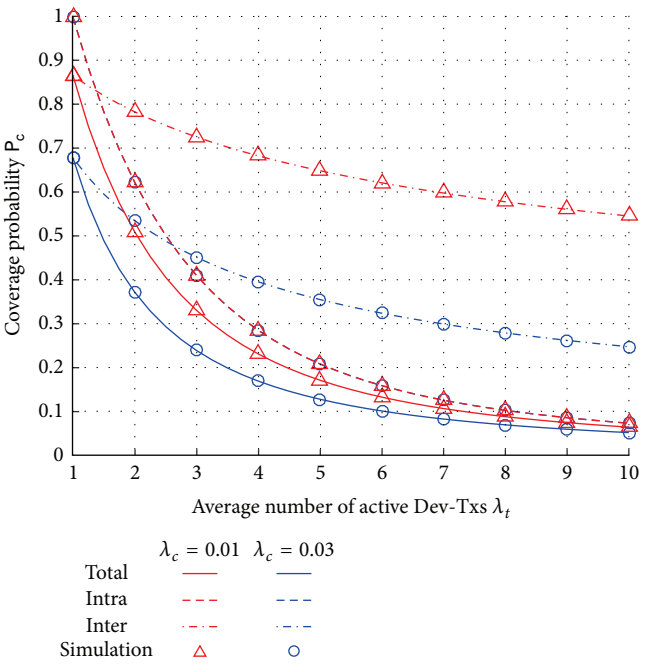

FIGURE 4: P_c versus λ_t with $\beta = 0$ dB, $\sigma = 0.5$, and $\lambda_c = \{0.01, 0.03\}$ clusters/m^3.

As shown in Figures 2, 3, and 4, we can observe the great correlation between the simulation and theoretical results. If comparing the curves with $\sigma = 0.3$ and 0.5 with the same λ_c in Figure 5, ASE increases, as σ decreases, which is expected from the result of P_c in Figure 3. Moreover, for the fixed $\sigma = 0.5$, the curves with $\lambda_c = 0.03$ show significantly higher ASE compared to the curve with $\lambda_c = 0.01$, because of the greater multiplication factor in (15). In Figure 6, the higher β makes ASE increase for small λ_t, while the curves with higher β decrease more rapidly compared to the curves with smaller β, as λ_t increases. One of the most important design aspects is the optimal λ_t to maximize the ASE, which determines network operation and wireless resource allocation. In Figure 5, $\lambda_t \approx 2$ gives the best ASE for all the three curves, which indicates its low sensitivity to σ and λ_c. On the other hand, if we increase the SIR threshold

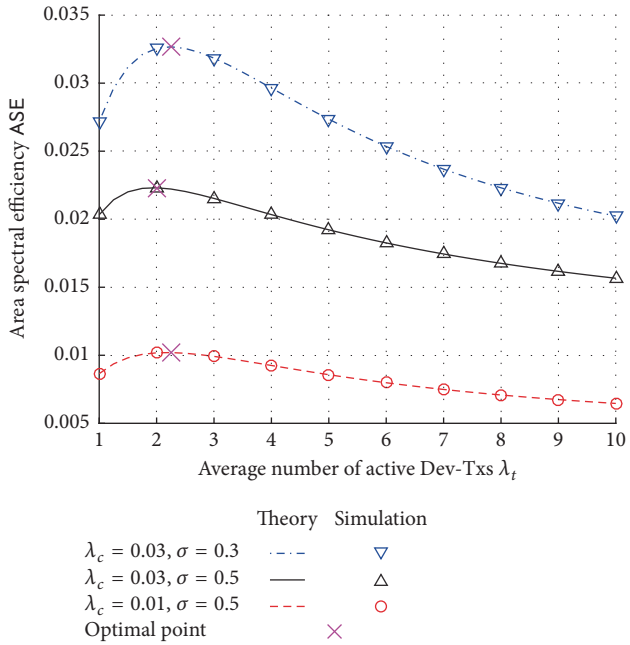

FIGURE 5: ASE versus λ_t; variations in σ and λ_c with $\beta = 0$ dB.

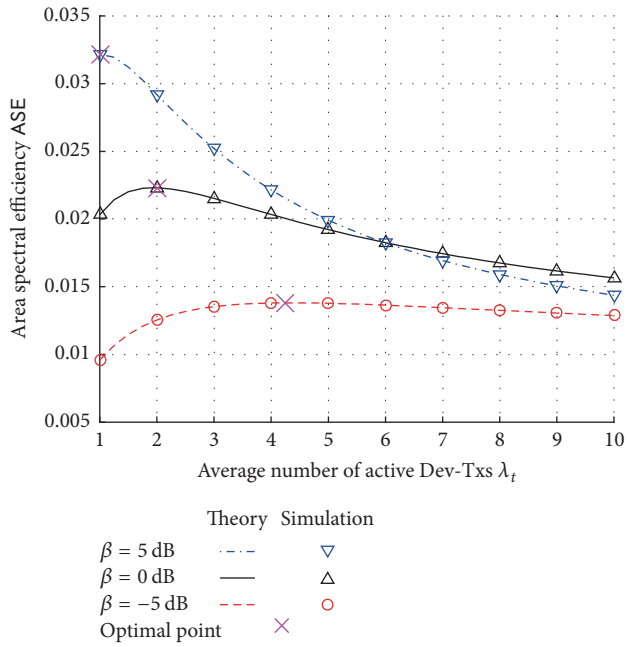

FIGURE 6: ASE versus λ_t with $\sigma = 0.5$, $\lambda_c = 0.03$ clusters/m^3, and $\beta = \{-5, 0, 5\}$ dB.

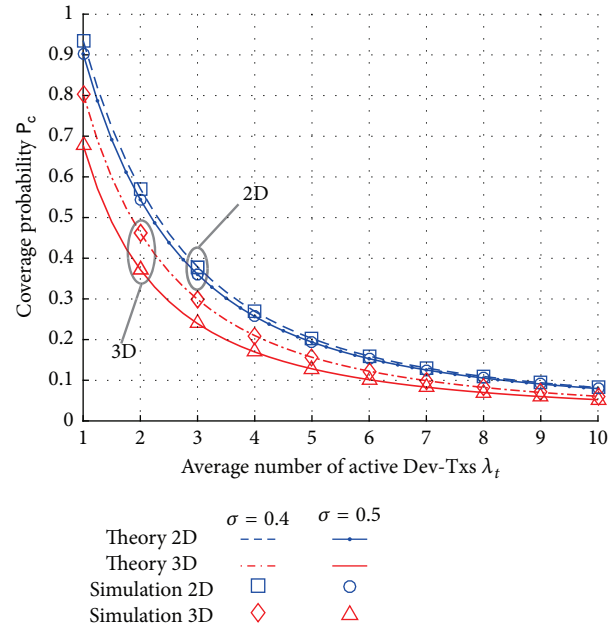

FIGURE 7: Comparison of 2D and 3D with $\beta = 0$ dB, $\lambda_c = 0.03$, and $\sigma = \{0.4, 0.5\}$.

β as in Figure 6, the optimal value of λ_t decreases (4.25, 2, 1 for $\beta = -5, 0, 5$ dB, resp.), because lower β can accommodate more simultaneous users (devices).

6.2. Comparison between 2D and 3D TCP Models. In this section, we compare the performance of the 3D clustered D2D networks with the 2D clustered networks studied in [12]. For the comparison, we set the same cluster density per unit space λ_c (clusters/m^2 and clusters/m^3 in 2D and 3D spaces, resp.). Figures 7 and 8 show the coverage probability P_c versus the average number of simultaneously active Dev-Txs λ_t in the 2D and 3D spaces. In the figures, the lined curves represent the theoretical results, while the markers indicate the simulation results. As shown in the figure, we observe that the analytical and simulation results are consistent with each other both for the 2D and 3D cases. For the same parameter set, P_c of the 2D TCP is higher compared to P_c of the 3D TCP, which is consistent with the results assuming uniform node distribution following PPP in [20]. This can be explained by more number of interferers inside volumes with the same radius from the typical device in 3D space compared to 2D space even with the same cluster density λ_c per unit space. From the figure, the gap between the 2D and 3D curves grows for the larger σ and λ_c. Furthermore, compared to the 3D space results, the P_c performances in the 2D space are less sensitive to the change in σ and λ_c as observed in Figures 7 and 8, respectively.

Furthermore, Figure 9 displays the area spectral efficiency ASE versus λ_t graphs of the 2D TCP under the change in β using the same parameters as the 3D TCP case shown in Figure 6: $\sigma = 0.5$, $\lambda_c = 0.03$ clusters/m^2, and $\beta = \{-5, 0, 5\}$ dB. Overall, the ASE in the 2D TCP is greater compared to the 3D case, because of the higher coverage probability P_c as indicated in Figures 7 and 8. That is, if we use the 2D TCP model for ultra-dense urban environments where the devices exist in 3D space, which will be common in the future wireless networks, both the coverage probability and the area spectral efficiency are overestimated. When comparing the impact of β, we can observe the similar trend in the 2D and 3D models that the higher β gives the higher ASE with small λ_t. However, while the curves with $\beta = 0$ dB and 5 dB cross over at around

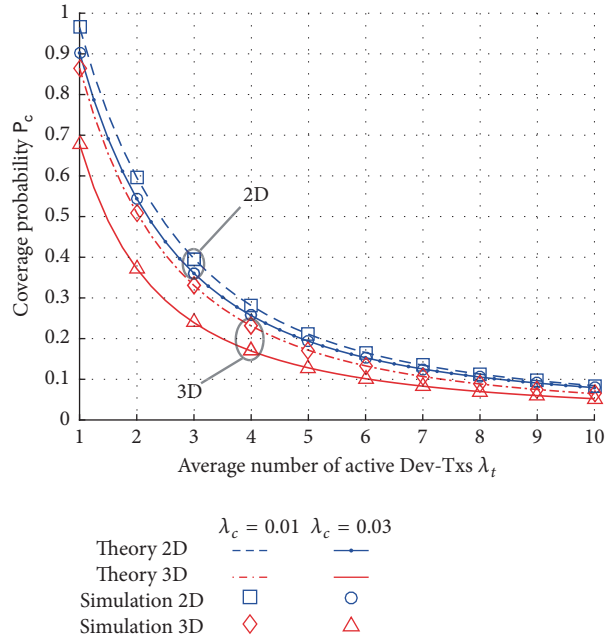

Figure 8: Comparison of 2D and 3D with $\beta = 0$ dB, $\sigma = 0.5$, and $\lambda_c = \{0.01, 0.03\}$.

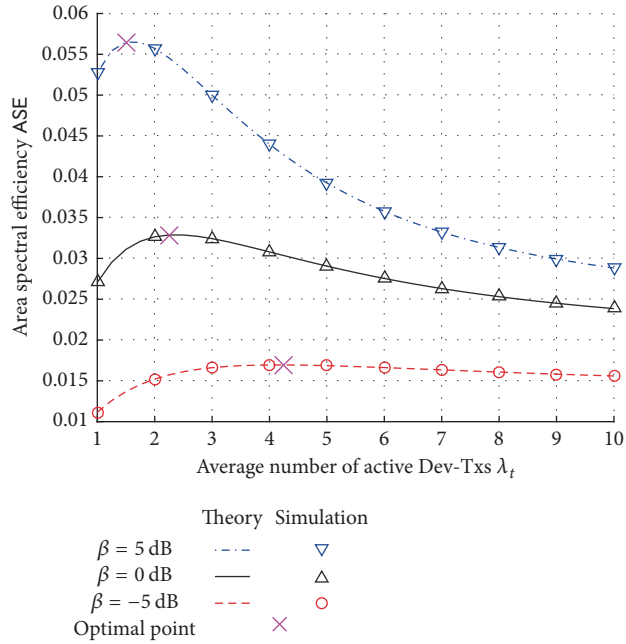

Figure 9: ASE versus λ_t in two-dimensional (2D) space with $\sigma = 0.5$, $\lambda_c = 0.03$ clusters/m^2, and $\beta = \{-5, 0, 5\}$ dB.

$\lambda_t = 6$ in Figure 6, the two curves in Figure 9 keep the measurable gap. Interestingly, the optimal λ_t to maximize the ASE shows the similar (but not exactly the same) trend to that seen in Figure 6. Thus, in a nutshell, the 2D TCP model can be used to estimate the optimal number of simultaneously active Dev-Txs in the 3D clustered networks; however both P_c and ASE estimated based on the 2D model are significantly overestimated compared to the actual performances of the 3D clustered D2D networks.

7. Conclusion

In this paper, we have studied clustered D2D networks in 3D space modeled by TCP for dense urban environments, where devices are distributed over the 3D space. Using stochastic geometry, we have analyzed P_c and ASE of the D2D network in the presence of cochannel interference from both the same cluster and the other clusters. We have derived the exact mathematical expressions of P_c and ASE, which were verified with the simulation results. Moreover, the approximate upper

and lower bounds on $\mathtt{P_c}$ have been derived, which provide design insights. Both the numerical and simulation results indicate that $\mathtt{P_c}$ in 3D space is significantly lower compared to 2D space for the same cluster density λ_c per unit space because of the more interferers within a certain distance. In addition, compared to the 3D space, the 2D TCP model is less sensitive to the system parameters such as the spatial scattering of the devices σ and the cluster density λ_c. Comparing the two models, we can conclude that the optimal numbers of simultaneously active devices λ_t to maximize ASE can be similar in the 2D and 3D models. However, it is not appropriate to use the 2D TCP to estimate $\mathtt{P_c}$ and ASE of the D2D networks following the 3D TCP especially for the large σ and λ_c.

The study in this paper provides guidelines on how to operate D2D networks in the presence of cochannel interference among devices, which are distributed in clusters in 3D space. The most significant aspect is how much simultaneous traffic to accommodate using the same channel. Through analysis and simulation, we have shown that there exist an optimal number of the simultaneously active D2D links to maximize ASE, and the optimum is smaller in the 3D D2D networks compared to the 2D D2D networks. Based on this result, one can determine the number of the cochannel D2D pairs to allow communicating in each cluster at the same time, which impacts the higher layer design such as wireless resource allocation for given cluster density λ_c, spatial scattering of devices σ, and quality of service (QoS) requirement characterized by β.

Appendix

A. Proof of Lemma 4

$$
\begin{aligned}
&\mathscr{L}_{I_{\text{intra}}}(s)\\
&= \int_{\mathbb{R}^3} \exp\left(\int_{\mathbb{R}^3} \frac{(1-\lambda_t) f_Y(y)\, dy}{1+\|y+x_0\|^{\alpha}/s}\right) \cdot f_Y(x_0)\, dx_0\\
&= \int_{\mathbb{R}^3} \exp\left(\int_{\mathbb{R}^3} \frac{(1-\lambda_t)}{1+\|z\|^{\alpha}/s} f_Y(z-x_0)\, dz\right)\\
&\quad \cdot f_Y(x_0)\, dx_0\\
&\overset{(a)}{\geq} \exp\left(\int_{\mathbb{R}^3}\int_{\mathbb{R}^3} \frac{(1-\lambda_t)}{1+\|z\|^{\alpha}/s} f_Y(z-x_0) f_Y(x_0)\, dx_0 dz\right)\\
&\overset{(b)}{\geq} \exp\left(\int_{\mathbb{R}^3} \frac{(1-\lambda_t)}{1+\|z\|^{\alpha}/s} \|f_Y * f_Y\|_{\infty}\, dz\right)\\
&= \exp\left(\frac{(1-\lambda_t)}{8\pi\sqrt{\pi}\sigma^3}\int_{\mathbb{R}^3} \frac{1}{1+\|z\|^{\alpha}/s} dz\right)\\
&= \exp\left[\frac{1-\lambda_t}{6\sqrt{\pi}\sigma^3}\frac{s^{3/\alpha}(3\pi/\alpha)}{\sin(3\pi/\alpha)}\right],
\end{aligned}
\tag{A.1}
$$

which corresponds to $\mathscr{L}^{*}_{I_{\text{intra}}}(s)$ in (17). (a) follows from Jensen's inequality, and (b) follows from Holder's inequality.

B. Proof of Lemma 5

$$
\begin{aligned}
&\mathscr{L}_{I_{\text{inter}}}(s)\\
&\overset{(a)}{\geq} \exp\left(4\pi\lambda_c \int_0^{\infty}\int_0^{\infty} \frac{-\lambda_t s u^{-\alpha}}{1+s u^{-\alpha}} f_U(u \mid v)\, du v^2 dv\right)\\
&\overset{(b)}{=} \exp\left(-4\pi\lambda_c\lambda_t \int_0^{\infty} \frac{s u^{-\alpha}}{1+s u^{-\alpha}} u^2 du\right)\\
&= \exp\left[-\frac{4}{3} s^{3/\alpha} \frac{\lambda_c\lambda_t\left(3\pi^2/\alpha\right)}{\sin(3\pi/\alpha)}\right],
\end{aligned}
\tag{B.1}
$$

which is $\mathscr{L}^{*}_{I_{\text{inter}}}(s)$ in (18). (a) follows from the Taylor expansion of an exponential function, and (b) is based on the property of the PDF in (10) that $\int_0^{\infty} f_U(u \mid v) v^2 dv = u^2$.

Conflicts of Interest

The authors declare that they have no conflicts of interest.

Acknowledgments

This research was supported by Basic Science Research Program through the National Research Foundation of Korea (NRF) funded by the Ministry of Education, Science and Technology (Grant no. 2016R1D1A1B03930060).

References

[1] F. Boccardi, R. W. Heath, A. Lozano, T. L. Marzetta, and P. Popovski, "Five disruptive technology directions for 5G," *IEEE Communications Magazine*, vol. 52, no. 2, pp. 74–80, 2014.

[2] J. G. Andrews, S. Buzzi, and W. Choi, "What will 5G be?" *IEEE Journal on Selected Areas in Communications*, vol. 32, no. 6, pp. 1065–1082, 2014.

[3] A. Asadi, Q. Wang, and V. Mancuso, "A survey on device-to-device communication in cellular networks," *IEEE Communications Surveys and Tutorials*, vol. 16, no. 4, pp. 1801–1819, 2014.

[4] Y. Li and W. Wang, "Message dissemination in intermittently connected D2D communication networks," *IEEE Transactions on Wireless Communications*, vol. 13, no. 7, pp. 3978–3990, 2014.

[5] S. Mumtaz, K. M. S. Huq, M. I. Ashraf, J. Rodriguez, V. Monteiro, and C. Politis, "Cognitive vehicular communication for 5G," *IEEE Communications Magazine*, vol. 53, no. 7, pp. 109–117, 2015.

[6] M. R. Palattella, M. Dohler, A. Grieco et al., "Internet of things in the 5G era: enablers, architecture, and business models," *IEEE Journal on Selected Areas in Communications*, vol. 34, no. 3, pp. 510–527, 2016.

[7] B. Bangerter, S. Talwar, R. Arefi, and K. Stewart, "Networks and devices for the 5G era," *IEEE Communications Magazine*, vol. 52, no. 2, pp. 90–96, 2014.

[8] O. Bello and S. Zeadally, "Intelligent device-to-device communication in the internet of things," *IEEE Systems Journal*, vol. 10, no. 3, pp. 1172–1182, 2014.

[9] M. Haenggi, *Stochastic Geometry for Wireless Networks*, Cambridge University Press, Cambridge, UK, 2012.

[10] H. Jung and I.-H. Lee, "Outage analysis of millimeter-wave wireless backhaul in the presence of blockage," *IEEE Communications Letters*, vol. 20, no. 11, pp. 2268–2271, 2016.

[11] H. Jung and I. Lee, "Outage Analysis of Multihop Wireless Backhaul Using Millimeter Wave under Blockage Effects," *International Journal of Antennas and Propagation*, vol. 2017, Article ID 4519365, 9 pages, 2017.

[12] M. Afshang, H. S. Dhillon, and P. H. Joo Chong, "Modeling and performance analysis of clustered device-to-device networks," *IEEE Transactions on Wireless Communications*, vol. 15, no. 7, pp. 4957–4972, 2016.

[13] H. Jung and I.-H. Lee, "Connectivity Analysis of millimeter-wave device-to-device networks with blockage," *International Journal of Antennas and Propagation*, vol. 2016, Article ID 7939671, 9 pages, 2016.

[14] M. Cha, H. Kwak, P. Rodriguez, Y. Y. Ahnt, and S. Moon, "I tube, you tube, everybody tubes: analyzing the world's largest user generated content video system," in *Proceedings of the ACM SIGCOMM Internet Measurement Conference*, pp. 1–14, October 2007.

[15] X. Cheng, C. Dale, and J. Liu, "Statistics and social network of YouTube videos," in *Proceedings of the 16th International Workshop on Quality of Service (IWQoS '08)*, pp. 229–238, IEEE, Enschede, The Netherlands, June 2008.

[16] T. Koskela, S. Hakola, T. Chen, and J. Lehtomäki, "Clustering concept using device-to-device communication in cellular system," in *Proceedings of the IEEE Wireless Communications and Networking Conference 2010, WCNC 2010*, pp. 1–6, April 2010.

[17] Y. Zhang, E. Pan, L. Song, W. Saad, Z. Dawy, and Z. Han, "Social network aware device-to-device communication in wireless networks," *IEEE Transactions on Wireless Communications*, vol. 14, no. 1, pp. 177–190, 2015.

[18] M. Ji, G. Caire, and A. F. Molisch, "Wireless device-to-device caching networks: basic principles and system performance," *IEEE Journal on Selected Areas in Communications*, vol. 34, no. 1, pp. 176–189, 2016.

[19] A. K. Gupta, X. Zhang, and J. G. Andrews, "Potential throughput in 3D ultradense cellular networks," in *Proceedings of the 49th Asilomar Conference on Signals, Systems and Computers, ACSSC 2015*, pp. 1026–1030, usa, November 2015.

[20] Z. Pan and Q. Zhu, "Modeling and analysis of coverage in 3-d cellular networks," *IEEE Communications Letters*, vol. 19, no. 5, pp. 831–834, 2015.

[21] A. Omri and M. O. Hasna, "Modeling and performance analysis of D2D communications with interference management in 3-D HetNets," in *Proceedings of the 59th IEEE Global Communications Conference, GLOBECOM 2016*, pp. 1–7, December 2016.

[22] Z. Pan and Q. Zhu, "Energy efficiency optimization in 3-D small cell networks-based sleep strategy," *IEEE Communications Letters*, vol. 21, no. 5, pp. 1131–1134, 2017.

[23] G. E. Andrews, R. Askey, and R. Roy, *Special Functions*, Cambridge University Press, Cambridge, UK, 1999.